Available online at www.sciencedirect.com
ScienceDirect
Journal of Solid State Chemistry 181 (2008) 1155–1166
JOURNAL OF SOLID STATE CHEMISTRY
www.elsevier.com/locate/jssc

Structural characterization and ferroelectric ordering in $(C_3N_2H_5)_5Sb_2Br_{11}$

A. Piecha[a], A. Pietraszko[b], G. Bator[a], R. Jakubas[a,*]

[a]*Faculty of Chemistry, University of Wrocław, Joliot–Curie 14, 50-383 Wrocław, Poland*
[b]*Institute of Low Temperature and Structure Research, Polish Academy of Science, Okólna 2, 50-950 Wrocław 2, PO Box 937, Poland*

Received 22 November 2007; received in revised form 11 February 2008; accepted 18 February 2008
Available online 4 March 2008

Abstract

A ferroelectric crystal $(C_3N_2H_5)_5Sb_2Br_{11}$ has been synthesized. The single crystal X-ray diffraction studies (at 300, 155, 138 and 121 K) show that it is built up of discrete corner-sharing bioctahedra $Sb_2Br_{11}^{5-}$ and highly disordered imidazolium cations. The room temperature crystal structure has been determined as monoclinic, space group, $P2_1/n$ with: $a = 9.139$ Å, $b = 15.150$ Å and $c = 13.969$ Å and $\beta = 96.19^\circ$. The crystal undergoes three solid–solid phase transitions: (*tetragonal*?) $\overset{354/352}{\longleftrightarrow} P2_1/n$ (**I** ↔ **II**) discontinuous, $P2_1/n \overset{145}{\longleftrightarrow} Pn$ (**II** ↔ **III**) continuous and $Pn \overset{120/135}{\longleftrightarrow} Pn$ (**III** ↔ **IV**) discontinuous. The dielectric and pyroelectric measurements allow us to characterize the low temperature phases **III** and **IV** as ferroelectric with the Curie point at 145 K and the saturated spontaneous polarization value of the order of 1.8×10^{-3} C m^{-2} along the *a*-axis (135 K). The ferroelectric phase transition mechanism at 145 K is due to the dynamics of imidazolium cations.

PACS: 77.80.−e; 77.70.+a; 61.10.−i

Keywords: Halogenoantimonate(III); Phase transition; Ferroelectric

1. Introduction

Halogenoantimonates(III) and halogenobismuthates(III) of the general formula $R_aM_bX_{(3b+a)}$ (where *R* denotes the organic cation, *M* denotes metal Sb(III) or Bi(III) and *X* denotes halogen atom: Cl, Br, I) form a promising group of materials from the point of view of nonlinear dielectric properties [1–3]. Numerous structural studies have showed that these metal halide complex salts are characterized by a rich diversity of the anionic structure [4,5]. The structure of the anionic moieties plays a crucial role in the generation of polar properties. It was shown that ferroelectricity have some tendency to appear in compounds characterized by two-dimensional anionic layers $(M_2X_9^{3-})_\infty$, (five salts). Four ferroelectric salts were found to crystallize in $R_5M_2X_{11}$ composition, for which anionic moieties constitute discrete bioctahedral units $Bi_2X_{11}^{5-}$ [6–10]. The origin of the ferroelectricity of either $R_3M_2X_9$ or $R_5Bi_2X_{11}$ subclass is ascribed to the dynamical disorder of dipolar organic cations as well as to an enhanced polarizability of the anionic sublattice.

The $R_5M_2X_{11}$ salts evoke much interest because the dielectric properties of the $(CH_3NH_3)_5Bi_2X_{11}$ salts (ferroelectrics at room temperature) were found to be comparable to those found in well-known TGS-family (TGS—tri-glycine sulfate) of crystals. Two another salts from this subgroup comprising in the structure aromatic cations, pyridinium or imidazolium, exhibit the ferroelectric properties at low temperatures: $((C_5H_5NH)_5Bi_2Br_{11} - T_c = 118$ K [10], $(C_3N_2H_5)_5Bi_2Cl_{11} - T_c = 166$ K [11]). The latter crystal was found to undergo two solid–solid phase transitions: $P\bar{4}n2 \overset{360\,K}{\longrightarrow} P2_1/n$ (**I** → **II**) discontinuous and $P2_1/n \overset{166\,K}{\longrightarrow} P2_1$ (**II** → **III**) continuous. The spontaneous polarization of the order of 6×10^{-3} C m^{-2} is characteristic of weak ferroelectrics. It is intriguing, that all known up till now salts crystallizing with $R_5M_2X_{11}$ (*M*-limited to Bi

*Corresponding author. Fax: +48 713282228.
E-mail address: rj@wchuwr.chem.uni.wroc.pl (R. Jakubas).

0022-4596/$ - see front matter © 2008 Elsevier Inc. All rights reserved.
doi:10.1016/j.jssc.2008.02.029

atom) chemical composition reveal, as a rule, ferroelectric properties. Thus, we extended our studies on molecular-ionic derivatives with $R_5M_2X_{11}$ composition containing in the crystal structure small heteroaromatic cations. We succeeded in obtaining, for the first time, halogenoantimonate(III) compound built up of discrete $Sb_2Br_{11}^{5-}$ anions namely: $(C_3N_2H_5)_5Sb_2Br_{11}$. In this article, we present the results of single crystal X-ray measurements (at 300, 155, 138 and 121 K), calorimetric, dielectric and pyroelectric studies on the ferroelectric compound $(C_3N_2H_5)_5Sb_2Br_{11}$. The mechanism of the paraelectric–ferroelectric phase transition in this compound is discussed.

2. Experimental

The starting materials were commercial $SbBr_3$ and imidazole amine ($C_3N_2H_4$). $[(C_3N_2H_5)]_5[Sb_2Br_{11}]$ crystals were prepared by dissolving stoichiometric amounts of $SbBr_3$ and imidazole in the concentrated HBr solution (molar ratio 2.5–1). The crystalline product was twice recrystallized. Single crystals were grown by slow evaporation from an aqueous solution.

Differential scanning calorimetry (DSC) runs were recorded with a Perkin Elmer DSC-7 in the temperature range 100–450 K. The TGA and DTA measurements were performed on a Setaram SETSYS 16/18 instrument between 300 and 500 K with a ramp rate of $2\,K\,min^{-1}$. The scan was performed in flowing nitrogen (flow rate: $1\,dm^3\,h^{-1}$). The dilatometric measurements were carried out by a thermomechanical analyzer Perkin Elmer TMA-7 in the temperature range 100–400 K. The dimensions of the sample were of the order of $5 \times 3 \times 1\,mm^3$.

The complex dielectric permittivity $\varepsilon^* = \varepsilon' - i\varepsilon''$ was measured by the HP 4285A Precision LCR Meters in the frequency range between 20 Hz and 1 MHz and in the temperature range from 100 to 450 K. The dimensions of the sample were of the order of $5 \times 3 \times 1\,mm^3$. The overall error in estimation of the real and imaginary parts of the complex dielectric permittivity value was less than 5% and 10%, respectively.

The single crystal for the X-ray measurements was selected as a mono-domain one at room temperature by means of polarizing microscope. The X-ray diffraction data were collected using an automatic X-ray four-circle KUMA Diffraction diffractometer and a XCalibur diffractometer with CCD area detectors at 300, 155, 138 and 121 K temperature points. Graphite monochromated Mo$K\alpha$ radiation ($\lambda = 0.071073$ nm) was generated at 50 kV and 25 mA. A single image for 1° rotation around the ω axis was obtained during 30 s and the full set of X-ray diffraction in the 2θ angles was collected over the range from 3° to 93°. The intensities of the reflections were recorded in 1200 frames for 6 runs. The lattice parameters were calculated for refinement of positions all measured reflections. X-ray study was performed at high temperature range up to 400 K with a KUMA diffraction temperature stage, the temperature of which was stabilized within 0.5 K. In the low temperature region, down to 80 K, the Oxford Cryo-system was used. Data reduction was performed using the CrysAlis Red program [12] with analytic absorption correction. The crystal structure at all temperature points was solved using the direct method—program SHELXL-97 [13]. The same program was used for the successive refinement cycles of the crystal structure. Crystallographic data (excluding structure factors) for the structure(s) reported in this paper have been deposited with the Cambridge Crystallographic Data Centre as supplementary publication no. CCDC 637536, 637537, 637538 and 637539. Copies of the data can be obtained free of charge on application to CCDC, 12 Union Road, Cambridge CB2 1EZ, UK (fax: +44 1223 336 033; e-mail: deposit@ccdc.cam.ac.uk).

3. Results and discussion

In order to characterize the thermal properties of $(C_3N_2H_5)_5Sb_2Br_{11}$ in a wide temperature region the DSC (100–450 K) and simultaneous TGA and DTA experiments (300–500 K) have been used.

Fig. 1(a) shows the DSC runs for $(C_3N_2H_5)_5Sb_2Br_{11}$ upon cooling and heating. Three solid–solid reversible phase transitions are disclosed. Above room temperature a strong heat anomaly (354/352 K, heating–cooling) corresponds to a discontinuous transition with an order–disorder mechanism, which is justified by a quite large transition entropy, ΔS_{tr} ca. $20\,J/mol\,K$. Below 300 K the crystal displays two phase transitions; the lowest temperature one at 120/135 K (cooling–heating, at a scanning rate of 1 K/min) is characterized by a significant temperature hysteresis ($\Delta T \approx 15$ K), which indicates its discontinuous nature ($\Delta S_{tr} = 4.2\,J/mol\,K$). The shape of the higher temperature anomaly at 145 K and a lack of the temperature hysteresis is typical of a continuous transition. The TGA and DTA results are shown in Fig. 1(b). The first endotherm at 353 K corresponds to the structural phase transition recorded by DSC. From the insert in Fig. 1(b) it can be seen that the loss of mass, of the order of $0.3 \pm 0.1\%$, appears in the whole temperature range between 325 and 375 K and not at a very phase transition (354 K). The loss of mass is undoubtedly due to the loss of particles absorbed on the crystal surface. It proves that a thermal anomaly on the DTA curve at 354 K is assigned to a structural phase transition. The compound is thermally stable up to ca. 450 K, and above 500 K it decomposes continuously.

The single X-ray diffraction on $(C_3N_2H_5)_5Sb_2Br_{11}$ at several temperatures confirmed all polymorphic phase transitions. Table 1 summarizes the results for the structure in the centrosymmetric space group at 155 and 300 K (phase **II**) and in the noncentrosymmetric space groups at 138 K (phase **III**) and 121 K (phase **IV**).

Since the crystal lattice parameters were found to display a visible structural anomaly close to ca. 230–240 K (the results are presented below in the text) it seemed interesting

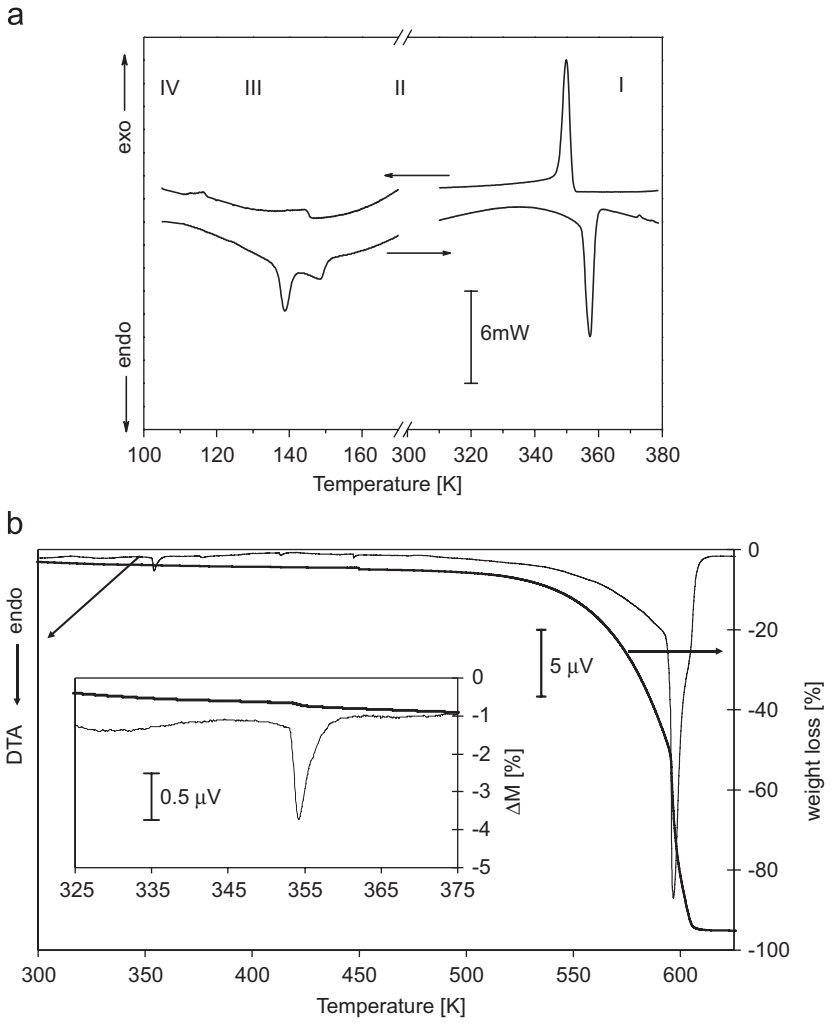

Fig. 1. (a) DSC curves for the $(C_3N_2H_5)_5Sb_2Br_{11}$ crystal upon cooling and heating runs (10 K/min, $m = 19.5$ mg). (b) Simultaneous TGA and DTA thermograms between 300 and 650 K.

to verify if we deal or not with a change in the symmetry of the crystal. The X-ray structure analysis at two temperatures, 155 and 300 K, clearly shows that there is no phase transition over this temperature interval. The X-ray studies confirm a continuous transition at 145 K from phase **II** to **III** and drastic structural discontinuous transition at 120 K to phase **IV**.

The data collected at 300, 155 and 138 K were recorded in the cooling cycle. The collected data at 121 K were obtained for the sample which was cooled down to 95 K and then heated up to 121 K. The systematic extinction rules indicated that the crystal structure belongs to the monoclinic symmetry with the space groups $P2_1/n$ both at 300 and 155 K and that the symmetry is described by the space group Pn for phases **III** and **IV** (at 138 and 121 K, respectively). The selected bond lengths and angles, limited to the geometry of the anion $Sb_2Br_{11}^{5-}$, are listed in Table 2. The asymmetric parts of $(C_3N_2H_5)_5Sb_2Br_{11}$, for the comparison at 155 and 121 K are shown in Figs. 2(a) and (b).

The projection of the crystal structure of $(C_3N_2H_5)_5Sb_2Br_{11}$ in the a-axis at 155 K is shown in Fig. 3. The polyhedra representation of the structure displayed in Fig. 4 show the mutual arrangement of the $M_2X_{11}^{5-}$ anions, which is characteristic of all ferroelectrics crystallizing with $R_5M_2X_{11}$ composition.

The crystal structure is built up of a discrete corner-sharing bioctahedra $Sb_2Br_{11}^{5-}$ and four kinds of symmetrically nonequivalent imidazolium cations. The bridging bromine atom (Br5) of the bioctahedral anionic units ($Sb_2Br_{11}^{5-}$) is located on an inversion center. Five imidazolium cations are divided into four nonequivalent kinds. The cations of type A placed in general positions are expected to be ordered in spite of enhanced displacement parameters. The other three cations, types B, C and D, occupy positions on an inversion center. All these cations were found to reveal a high dynamical disorder, which is described by a two-site model with the equal occupancy factors (0.5/0.5). An attempt of the splitting of the A cation into two parts in phase II was undertaken, it, however, did not affect the discrepancy factor R. In our opinion the enhanced atomic displacement parameters in phase II may be a result of a possible small-angle libration motion of the

Table 1
Crystal data and structure refinement for $[C_3N_2H_5]_5Sb_2Br_{11}$ at 121, 138, 155 and 300 K

Phase	121 K	138 K	155 K	300 K
Empirical formula	$(C_3N_2H_5)_5Sb_2Br_{11}$	$(C_3N_2H_5)_5Sb_2Br_{11}$	$(C_3N_2H_5)_5Sb_2Br_{11}$	$(C_3N_2H_5)_5Sb_2Br_{11}$
Formula weight ($g\,mol^{-1}$)	1467.96	1467.96	1467.96	1467.96
Temperature	121(2)	138(2)	155(2)	300(2)
Wavelength	0.71073	0.71073	0.71073	0.71073
Crystal system	Monoclinic	Monoclinic	Monoclinic	Monoclinic
Space group	*Pn*	*Pn*	$P2_1/n$	$P2_1/n$
a (Å)	9.114(19)	9.134(19)	9.170(19)	9.139(19)
b (Å)	15.165(3)	15.036(3)	15.038(3)	15.150(3)
c (Å)	13.781(3)	13.971(3)	13.939(3)	13.969(3)
β (°)	98.04(3)	98.56(3)	98.48(3)	96.19(3)
V (Å^3)	1886.07(7)	1897.6(7)	1901.1(7)	1923.0(7)
Z	2	2	2	2
Calculated density ($g\,cm^{-3}$)	2.585	2.569	2.564	2.535
Absorption coefficient (mm^{-1})	13.110	13.030	13.006	12.857
F(000)	1344	1344	1344	1344
Crystal size (mm)	0.28 × 0.24 × 0.21	0.28 × 0.24 × 0.21	0.28 × 0.24 × 0.21	0.28 × 0.24 × 0.21
Theta range for data collection (°)	3.94–28.09	3.95–28.13	3.94–28.14	3.98–28.50
Ranges of *h*, *k*, *l*	$-11\leqslant h\leqslant 11$ $-19\leqslant k\leqslant 19$ $-15\leqslant l\leqslant 18$	$-12\leqslant h\leqslant 12$ $-18\leqslant k\leqslant 19$ $-15\leqslant l\leqslant 18$	$-12\leqslant h\leqslant 12$ $-18\leqslant k\leqslant 19$ $-15\leqslant k\leqslant 18$	$-12\leqslant h\leqslant 12$ $-19\leqslant k\leqslant 19$ $-18\leqslant k\leqslant 16$
Reflections collected	18 275	18 685	18 685	18 448
Independent reflections R_{int}	0.0526	0.0578	0.0537	0.1077
Data/restraints/parameters	7053/62/345	7119/62/348	4369/28/242	4494/28/242
Goodness-of-fit on F^2	1.134	0.960	1.045	0.942
Final R_1/wR_2 indices ($I>2\sigma I$)	0.0438/0.0892	0.0383/0.0772	0.0354/0.0751	0.0382/0.0668
Largest diff. peak/hole (eÅ^{-3})	1.986/ − 1.486	1.146/ − 0.873	1.192/ − 1.094	0.933/ − 0.690

A cation. Disordered cations are able to perform the 180° reorientation within the plane of the pentagonal ring. The geometry of the bioctahedral unit $Sb_2Br_{11}^{5-}$ (see Table 2) is typical of those found so far in four other $R_5M_2X_{11}$ crystals.

Two models of the crystal structure at 138 K in the ferroelectric phase **III** were considered. For the first model including all the ordered imidazolium cations (*Pn* space group) a refinement with a discrepancy factor *R* equal to 3.8% was obtained, however, with very large displacement parameters of the B, C and D cations. The refinements of the crystal structure with disordered B, C and D imidazolium moieties showed the same *R* factor with the normal displacement coefficients. The population factors of two positions occupied by disordered B, C and D imidazolium cations for the one preferred was larger than 50%. After the phase transitions from phase **III** to phase **IV** the crystal structure is described by the monoclinic space group *Pn* but with fully ordered imidazolium cations. It should be noted, however, that the cation of type D, even at 121 K, is still characterized by an enhanced displacement coefficients. Thus, it may be split into two positions with a various occupancy (see Table 3 and Fig. 5). The phase transition (**III** → **IV**) is classified as an isomorphous transition. The results of analysis of the dynamic properties of all cations in three phases are collected in Table 3.

The crystal structure of $(C_3N_2H_5)_5Sb_2Br_{11}$ is characterized by a three-dimensional network of N-H···Br hydrogen bonds which are treated as weak bonds (see Table 4). At 300 K the shortest N-H···Br bonds are close to ca. 3.43 Å, but with temperature decreasing down to 155 K they contract by about 0.1 Å. The hydrogen-bonds system is nearly identical to that found in the $(C_3N_2H_5)_5Bi_2Cl_{11}$, however, the bonds in the bromine analog seem to be weaker, thus imidazolium cations are more loosely packed in the crystal lattice of $(C_3N_2H_5)_5Sb_2Br_{11}$.

It seems to be interesting to compare also the distortion of the $M_2X_{11}^{5-}$ bioctahedra in the two closely related compounds: methylammonium analog $(CH_3NH_3)_5Bi_2Cl_{11}$ and imidazolium one $(C_3N_2H_5)_5Sb_2Br_{11}$. Despite the structural similarities of both analogs their dielectric properties and phase situation are different ($T_c = 307$ K, $Pcab \rightarrow Pca2_1$, $P_s = 2.0\times10^{-2}\,C\,m^{-2}$ (Cl) and $T_c = 145$ K, $P2_1/n \rightarrow Pn$, $P_s = 1.8\times10^{-3}\,C\,m^{-2}$ (Br)). It was shown that the methylammonium analogs reveal a noticeable evolution in the "torsion angle" of the bioctahedral unit by nearly 14.5° over the ferroelectric phase [14]. It was suggested that this deformation could contribute to some extend to the origin of the spontaneous polarization. Unexpectedly, in the case of the imidazolium analog, this type of deformation (defined as an angle between two planes containing Br6, Sb1, Br5 and Br5, Sb1S, Br3S) (see Fig. 2) changes rather weakly with temperature: 0.39° (300 K), 0.27° (155 K), 0.49° (138 K) and 1.80° (121 K) giving the total value ca. 1.53°. A change in the corresponding angle for the atoms Br3, Sb1, Sb1S and Br6S is even smaller, ca. 0.6° between 300 and 121 K. It indicates that this type of distortion of the bioctahedral

Table 2
Selected bond lengths (Å) and angles (deg) for $[C_3N_2H_5]_5Sb_2Br_{11}$ at 121, 138, 155 and 300 K

	121 K	138 K	155 K	300 K
Sb(1)–Br(4)	2.6836(10)	2.6354(9)	2.6447(5)	2.6492(7)
Sb(1)–Br(2)	2.7144(11)	2.6930(10)	2.6671(7)	2.6717(9)
Sb(1)–Br(6)	2.7320(12)	2.7626(9)	2.7574(6)	2.7529(8)
Sb(1)–Br(3)	2.8833(12)	2.8710(10)	2.8579(6)	2.8048(9)
Sb(1)–Br(1)	2.9069(11)	2.9930(10)	2.9756(8)	2.9057(9)
Sb(1)–Br(5)	2.9379(12)	2.9953(16)	2.9865(5)	3.0248(5)
Br(5)–Sb(1)$^{(i)}$	–	–	2.9865(5)	3.0248(5)
Sb(1S)–Br(2S)	2.6292(11)	2.6498(9)	–	–
Sb(1S)–Br(4S)	2.6322(10)	2.6576(8)	–	–
Sb(1S)–Br(6S)	2.8166(11)	2.7460(9)	–	–
Sb(1S)–Br(3S)	2.7951(11)	2.8513(9)	–	–
Sb(1S)–Br(1S)	3.0729(9)	2.9592(10)	–	–
Sb(1S)–Br(5)	3.0344(12)	2.9840(16)	–	–
Br(4)–Sb(1)–Br(2)	89.01(3)	91.12(3)	91.70(2)	90.75(3)
Br(4)–Sb(1)–Br(6)	95.02(4)	92.50(3)	91.47(2)	91.24(3)
Br(2)–Sb(1)–Br(6)	91.55(3)	91.88(3)	90.88(17)	91.94(2)
Br(4)–Sb(1)–Br(3)	87.89(3)	91.14(3)	92.00(2)	90.99(3)
Br(2)–Sb(1)–Br(3)	91.87(3)	88.36(3)	89.24(17)	88.63(2)
Br(6)–Sb(1)–Br(3)	175.54(3)	176.35(3)	176.43(9)	177.70(2)
Br(4)–Sb(1)–Br(1)	89.73(3)	88.25(3)	87.92(2)	90.31(3)
Br(2)–Sb(1)–Br(1)	178.08(3)	178.04(2)	178.75(9)	178.51(2)
Br(6)–Sb(1)–Br(1)	87.11(3)	90.01(2)	90.31(16)	89.08(2)
Br(3)–Sb(1)–Br(1)	89.54(3)	89.79(2)	89.00(16)	90.31(2)
Br(4)–Sb(1)–Br(5)	172.94(4)	171.05(4)	171.15(8)	174.57(19)
Br(2)–Sb(1)–Br(5)	96.38(4)	97.82(4)	97.14(2)	94.65(2)
Br(6)–Sb(1)–Br(5)	89.40(4)	87.65(4)	87.92(19)	88.06(2)
Br(3)–Sb(1)–Br(5)	87.38(4)	88.71(4)	88.52(19)	89.67(2)
Br(1)–Sb(1)–Br(5)	85.00(3)	82.80(4)	83.26(2)	84.30(2)
Sb(1)$^{(i)}$–Br(5)–Sb(1)	–	–	180.00	180.00

Symmetry transformations used to generate equivalent atoms: (i) $-x$, $-y$, $-z+2$.

units in $(C_3N_2H_5)_5Sb_2Br_{11}$ is not as important as that in the $(CH_3NH_3)_5Bi_2Cl_{11}$ compound (see Fig. 3 in [14]). On the other hand the angle between two planes containing the following atoms: Br2S, Br3S, Br1S, Br6S, Sb1S and Br2, Br3, Br1, Br6, Sb1 reveal more distinct changes namely: 300 K (0°), 155 K (0°), 138 (0.25°) and 121 K (5.03°). It is clearly seen that paraelectric–ferroelectric transition (**II** → **III**) at 145 K is accompanied by a negligible distortion of anions, whereas in the lowest temperature transition **III** → **IV** at 120 K the anionic sublattice experiences drastic distortion. The crystal structure of the title compound is characterized by a presence of an extended system of weak hydrogen bonds forming approximately a three-dimensional network. The distortion of the bioctahedral units $Sb_2Br_{11}^{5-}$ reflects the interaction of the anionic and cation sublattices via the N−H···Br hydrogen bonds. Relatively small deformation of the $Sb_2Br_{11}^{5-}$ units through the paraelectric–ferroelectric transition at 145 K is rather unexpected. It means that the hydrogen bonds system in the title compound plays the minor role with respect to the possible origin of ferroelectricity in phase **III**. In contrast, in the methylammonium analogs the polarization of the N−H···Cl hydrogen bonds in the ferroelectric phase was believed to contribute to the electric spontaneous polarization P_s [14]. In turn, the lowest temperature phase transition **III** → **IV** in $(C_3N_2H_5)_5Sb_2Br_{11}$, most likely, is connected with a significant rebuilding in the three-dimensional network of hydrogen bonds configuration and consequently the change in the reorientation of polar cationic units. This effect, most probably an antiparallel alignment of dipolar cations, results in the rapid reduction of spontaneous polarization magnitude in the vicinity of **III** → **IV** ferroelectric–ferroelectric phase transition.

The dynamic dielectric response in the $(C_3N_2H_5)_5Sb_2Br_{11}$ crystal (presented below) leads to the conclusion that we deal with an "order-disorder" mechanism of the phase transition at 145 K. On the basis of the X-ray experiment we can state, without any doubts, that the changes in the motional state of the imidazolium cations play the crucial role in the phase transition mechanism. Thus, it seems interesting to compare the occupation magnitudes for two-site model of the imidazolium cations in various phases that was disclosed from the X-ray studies (see Table 3).

The cations labeled as A or AS (placed in general position) do not contribute to the spontaneous polarization (P_s), since they are ordered in all considered phases. The remaining three types B, C and D equally distributed over two positions in phase **II**, below $T_c = 145$ K have a tendency to occupy one position. In the ferroelectric phase exclusively the cations B and C contribute to the P_s value, whereas D one is still highly disordered. The full order of the cations B and C is not reached down to the **III** → **IV** transition temperature. In the lowest temperature phase **IV** most of the cations is practically ordered, with the exception of the D type, which is still partially disordered. We can state that the mechanism of the ferroelectric phase transition is rather complex, which is the common feature of all ferroelectric compound with the $R_3M_2X_{11}$ composition. Nevertheless, there is no doubt that the spontaneous polarization over phase **III** in $(C_3N_2H_5)_5Sb_2Br_{11}$ originates predominantly from the behavior of two of five imidazolium cations located in the crystal lattice.

Fig. 6(a) shows the lattice parameters a and c, whereas Fig. 6(b) the parameter b and monoclinic β angle vs. temperature over the temperature 90–300 K.

One can distinguish three characteristic points on the lattice parameters runs in the presented temperature region. At ca. 240 K there is observed a significant change in the linear part of the temperature characteristics of the a and b parameters and a well shaped minimum for the c-value. These structural anomalies at ca. 240 K suggest that the crystal structure experiences some important rebuilding, without any change in the space group, which is reflected in the calorimetric and dielectric studies. Unexpectedly, the ferroelectric phase transition at 145 K is rather hardly visible, nonetheless the dilation of the sample along the b-axis is better seen, showing a clear change in the sign of the linear thermal expansion coefficient approaching 145 K. On the other hand the lowest temperature phase transition at 120 K is accompanied by

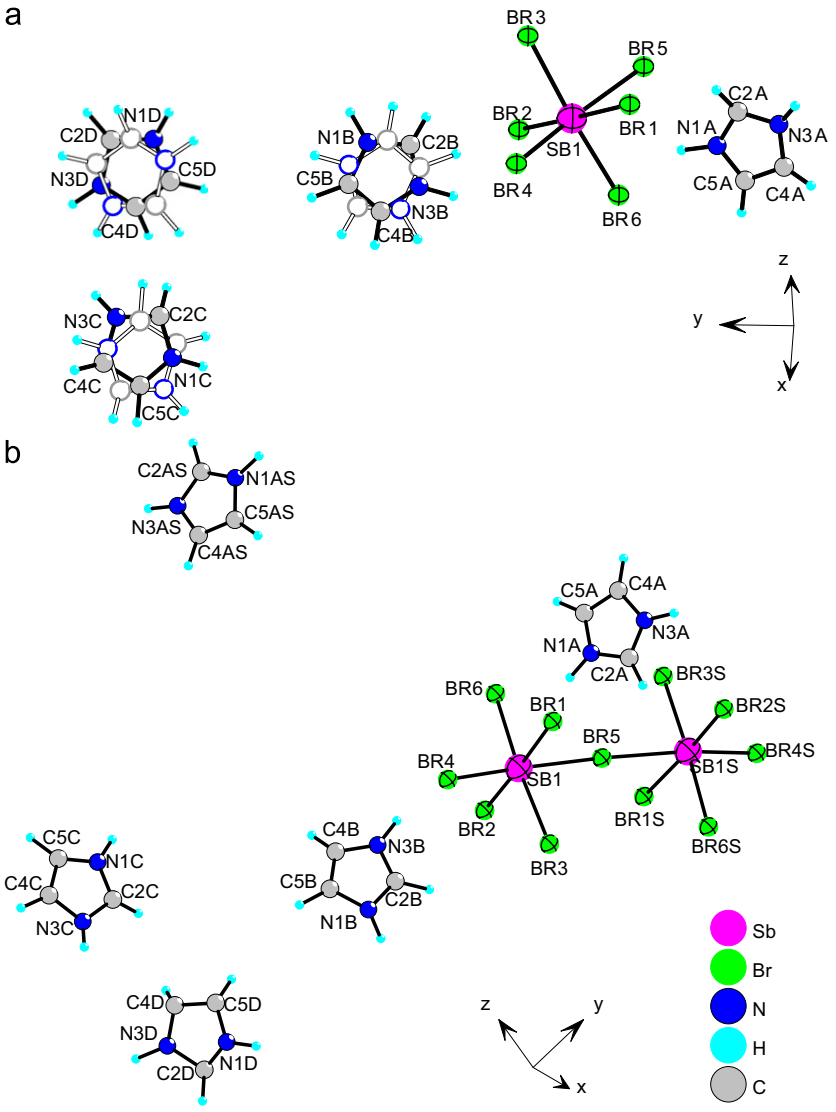

Fig. 2. Independent parts of the unit cell of $(C_3N_2H_5)_5Sb_2Br_{11}$ at 155 K (upper part) and 121 K (lower part) with the atom labeling scheme.

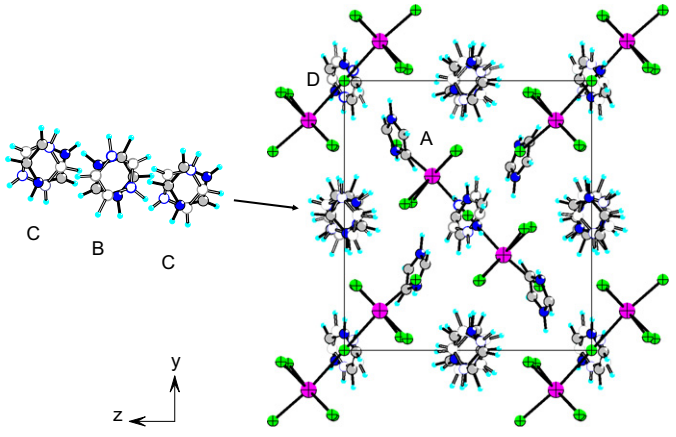

Fig. 3. Crystal packing down the *a*-axis in $(C_3N_2H_5)_5Sb_2Br_{11}$ in phase **II** at 155 K. Displacement ellipsoids are drawn at the 50% probability level.

an enormous rapid expansion (upon cooling) along the *b*-axis by ca. 0.6%, large compression along the *c*-direction by ca. 2.2% and an important drop in the monoclinic β angle from 98.5° to 98°. It should be also added that over the studied temperature region the angle changes by nearly 3° which indicates a significant distortion of the crystal structure through the **III** → **IV** phase transition. The relative change in the unit cell volume, $\Delta V/V$, at 120 K was estimated to be ca. 4.2×10^{-3}. The preliminary X-ray studies show that the title crystal, most likely, changes its symmetry above 354 K from monoclinic to tetragonal.

The optical observations under the polarizing microscope for $(C_3N_2H_5)_5Sb_2Br_{11}$ disclosed a ferroelastic domain structure in the room temperature phase. Unfortunately, the expected paraelastic phase (prototypic) could not be verified since close to the high temperature phase transition (**II** → **I**) the single crystal becomes nontransparent due to some changes on its surface.

It should be added that during the **III** → **IV** phase transition the ferroelastic domain structure does not change its pattern. Similarly, the monodomain single crystals (at room temperature) taken for X-ray studies does not show any twinning through the **III** → **IV** phase

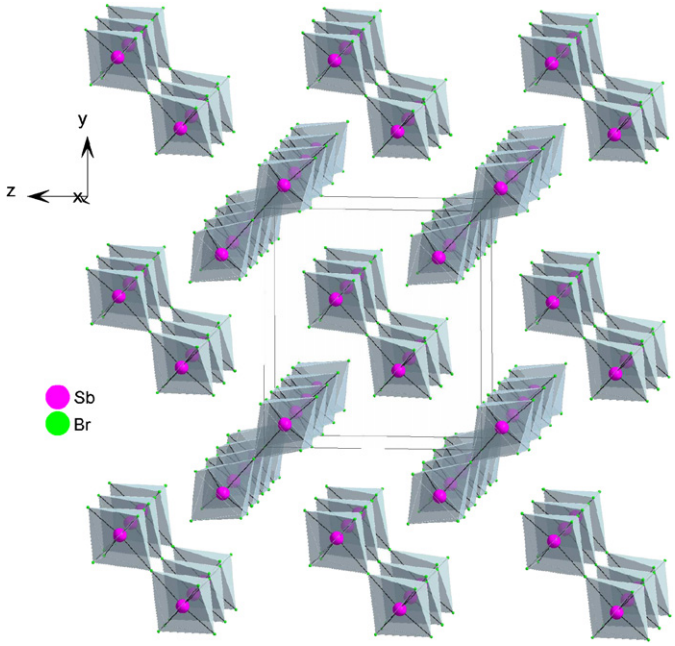

Fig. 4. View of $(C_3N_2H_5)_5Sb_2Br_{11}$ as a polyhedral representation (approximately along the *a*-direction).

Table 3
The dynamic properties of imidazolium cations in various phases (the occupancy factors of the preferred positions for two-site model)

Type of cation	Temperature (K)		
	121 K (phase **IV**)	138 K (phase **III**)	155 K (phase **II**)
A (AS)	100%	100%	100%
B	92%	67%	50%
C	83%	66%	50%
D	71%	55%	50%

transition, despite of the fact, that this transition is accompanied by a drastic changes in the crystal lattice parameters.

The X-ray studies revealed that two isomorphous at room temperature imidazolium analogs ($P2_1/n$), $(C_3N_2H_5)_5Bi_2Cl_{11}$, $(C_3N_2H_5)_5Sb_2Br_{11}$, underwent to phase with a different space groups in their low temperature ferroelectric phases, 2_1 and *Pn*, respectively. It means that the polar axis in each compound are mutually perpendicular. To confirm it and verify the propriety of the choice of the *Pn* space group below 145 K for $(C_3N_2H_5)_5Sb_2Br_{11}$ we carried out the measurements of ε' for samples cut from the same single crystals along various directions. Dielectric measurements performed for six crystallographically independent directions allowed us to estimate the dielectric permittivity tensor. The representation of the tensor in the principal axes system close to 145 K is given below:

$$\begin{bmatrix} 306 & 0 & 0 \\ 0 & 65 & 0 \\ 0 & 0 & 43 \end{bmatrix} \quad (1)$$

Table 4
Hydrogen bonds in $[C_3N_2H_5]_5Sb_2Br_{11}$ (Å) and (deg) at 300, 155, 138 and 121 K

$D-H\cdots A$	$d(D\text{-}H)$	$d(H\cdots A)$	$d(D\cdots A)$	$<(DHA)$
300 K				
N(1A)-H(1A)...Br(6)	1.05	2.49	3.418(5)	147.5
N(3A)-H(3A)...Br(1)$^{(vii)}$	1.08	2.53	3.451(5)	142.4
N(1C)-H(1C)...*Br*(3)$^{(viii)}$	1.08	2.38	3.441(9)	165.2
N(3D)-H(1D)...*Br*(3)$^{(ix)}$	1.04	2.44	3.475(11)	171.0
155 K				
N(1A)-H(1A)...Br(6)	1.09	2.34	3.340(18)	152.3
N(3A)-H(3A)...Br(1)$^{(vii)}$	0.96	2.63	3.360(18)	132.4
N(1C)-H(1C)...*Br*(3)$^{(viii)}$	1.00	2.39	3.361(2)	165.6
N(3D)-H(3D)...*Br*(3)$^{(ix)}$	1.10	2.49	3.563(3)	166.3
138 K				
N(1B)-H(1B)...Br(1)$^{(i)}$	1.05	2.56	3.357(2)	132.4
N(3B)-H(3B)...Br(1S)$^{(ii)}$	1.05	2.42	3.390(3)	152.4
N(3D)-H(3D)...Br(1)$^{(iii)}$	1.05	2.69	3.600(2)	144.3
N(1AS)-H(1AS)...Br(6S)$^{(iv)}$	1.05	2.43	3.310(3)	141.3
N(1A)-H(1A)...Br(6)	1.05	2.51	3.385(3)	140.4
N(3A)-H(3A)...Br(1S)$^{(v)}$	1.05	2.51	3.370(3)	138.3
N(3AS)-H(3AS)...Br(1)$^{(vi)}$	1.05	2.31	3.323(3)	160.6
N(1C)-H(1C)...Br(3S)$^{(ii)}$	1.05	2.34	3.348(3)	159.2
N(1D)-H(1D)...Br(3)$^{(vi)}$	1.05	2.52	3.545(3)	166.1
121 K				
N(1B)-H(1B)...Br(1)$^{(i)}$	1.05	2.49	3.342(14)	137.8
N(3B)-H(3B)...Br(1S)$^{(ii)}$	1.05	2.33	3.341(3)	161.1
N(3D)-H(3D)...Br(1)$^{(iii)}$	1.21	3.16	3.708(14)	107.2
N(1AS)-H(1AS)...Br(6S)$^{(iv)}$	1.05	2.30	3.264(17)	152.1
N(1A)-H(1A)...Br(6)	1.05	2.48	3.391(16)	144.1
N(3A)-H(3A)...Br(1S)$^{(v)}$	1.05	2.48	3.423(16)	149.1
N(3AS)-H(3AS)...Br(1)$^{(vi)}$	1.05	2.37	3.274(18)	143.2
N(1C)-H(1C)...Br(3S)$^{(ii)}$	1.05	2.28	3.295(3)	163.1

Symmetry transformations used to generate equivalent atoms: (i) $x-1/2$, $-y+1$, $-z+1/2$ (ii) $x-1/2$, $-y+1$, $z+1/2$, (iii) $x-1$, $y-1$, z (iv) $x-1$, y, $z+1$, (v) $x+1/2$, $-y+2$, $z+1/2$ (vi) $x-3/2$, $-y+1$, $z+1/2$, (vii) $-x-1/2$, $y-1/2$, $-z+3/2$ (viii) $-x+1/2$, $y+1/2$, $-z+3/2$, (ix) $x+1$, $y+1$, z.

The geometric interpretation of the permittivity tensor is an ellipsoid. The cross-section of the ellipsoid in the *ac* plane is presented as an ellipse in Fig. 7. The corresponding directional dependence of the electric permittivity, ε, is calculated according to the relationship

$$\varepsilon = \frac{1}{r^2} \quad (2)$$

where r is a distance from the origin of the Cartesian system, (0, 0), to the section with the ellipse in a specific direction. The directional dependence of ε is presented as a dotted line in Fig. 7. Particularly the direction of the largest value of ε is shown, which forms an angle of ca. $20^\circ \pm 3^\circ$ with the *a*-axis.

The direction of the largest value of the permittivity lies in the *ac* monoclinic plane at an angle of about 20° to the *a*-axis. This is consistent with the group-subgroup relation ($P2_1/n \rightarrow Pn$). This confirms the appropriate choice of the space group symmetry of the ferroelectric phase. In this

Table 5
Ferroelectric transitions in crystals with $R_5M_2X_{11}$ (M = Sb, Bi and X = Cl, Br) composition and their dielectric properties

Crystal	T_c (K)	Order PT	Symmetry change at T_c	P_s ($C\,m^{-2}$)	ε'_{max} (T_c)	Ref.
$(CH_3NH_3)_5Bi_2Cl_{11}$	307	II	$Pcab \rightarrow Pca2_1$	1.2×10^{-2}	8.0×10^3	[18]
$(CH_3NH_3)_5Bi_2Br_{11}$	311	II	$Pcab \rightarrow Pca2_1$	2.0×10^{-2}	2.0×10^4	[19,20]
$(C_5H_5NH)_5Bi_2Br_{11}$	118	II	$P2_1/n \rightarrow P2_1$	3.0×10^{-3}	2.2×10^2	[21]
$(C_3N_2H_5)_5Bi_2Cl_{11}$	166	II	$P2_1/n \rightarrow P2_1$	6.0×10^{-3}	4.5×10^2	[11]
$(C_3N_2H_5)_5Sb_2Br_{11}$	145	II	$P2_1/n \rightarrow P2_n$	1.8×10^{-3}	2.5×10^2	

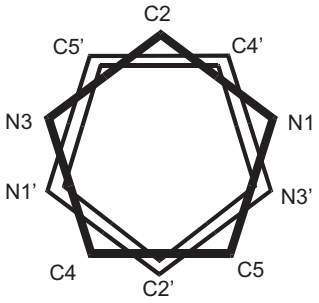

Fig. 5. Two possible positions (two-site model, 180°-reorientation) of the cations.

case the spontaneous polarization is expected to appear within the *ac* plane.

The temperature dependence of the complex dielectric permittivity ($\varepsilon^* = \varepsilon' - i\varepsilon''$) along the *a*-axis was measured between 20 Hz and 1 MHz upon cooling. The real part of ε^* is presented for two selected frequencies, 135 Hz and 1 MHz, to illustrate the dielectric response in the vicinity of the low temperature transitions at 145 and 120 K (see Fig. 8).

$\varepsilon'_{a(max)}$ reaches ca. 245 units (135 Hz) at 145 K, whereas the anomaly accompanying the transition **III** → **IV** hardly visible at the frequency of 135 Hz, is clearly seen at 1 MHz (see the inset in Fig. 7). The temperature dependence of the dielectric permittivity, ε'_a, close to 145 K strongly suggests ferroelectric character of the **II** → **III** transition. The low frequency dielectric studies disclosed a relaxation process around 145 K with the critical slowing down of the macroscopic relaxation time characteristic of ferroelectric materials with an order–disorder mechanism. The full analysis of dynamic dielectric response for the paraelectric-ferroelectric transition in $(C_3N_2H_5)_5Sb_2Br_{11}$ has been reported recently [15]. The Curie–Weiss formula, $\varepsilon'_{a(135\,Hz)} = C \pm /(T - T_c)$, is well fulfilled over the temperature interval of ca. 5 K both above and below T_c = 145 K (Fig. 9).

It should be emphasized that the ratio $C_+/C_- = 1.82$, which is quite close to the theoretical value ($C_+/C_- = 2$) expected for the second order ferroelectric phase transition. Nevertheless, we should remember that the lowest frequency of the measuring electric field of 135 Hz used in our experiment is in the dispersion frequency region, thus the ratio C_+/C_- may change with decreasing frequency.

The pyroelectric measurements were performed over two various temperature regions, since the title crystal experiences quite complex sequence of phase transitions at low temperatures. To characterize polar properties of the low temperature phases after poling of the crystal the pyroelectric effect should be recorded only upon heating scans. In turn, during heating scan, starting from the lowest temperature of phase **IV**, the transitions, **IV** → **III** and **III** → **II**, have a tendency to overlap. Thus, the pyroelectric current was measured after pooling the crystal from 150 down to ca. 130 K. The DC electric field was equal to about +8 kV/cm. Then the pyroelectric current $I_{pyr.}$ was measured with temperature increasing at the rate of 1 K/min. The same procedure was repeated after using the negative DC electric field of −8 kV/cm. The recorded spontaneous polarization, P_s as a function of temperature is illustrated in Fig. 10.

It is clearly seen that the spontaneous polarization is reversed by the external DC electric field. Such a behavior of P_s is a direct evidence that we deal with the ferroelectric properties of $(C_3N_2H_5)_5Sb_2Br_{11}$ below T_c (**II** → **III**). The saturated value of P_s obtained in phase **III**, just before reaching phase **IV** mounts $1.8 \times 10^{-3}\,C\,m^{-2}$ and is typical of "weak" ferroelectrics e.g. $Li_2Ge_7O_{15}$ [16], cyclohexane-1, 1′-diacetic acid [17]. According to the Landau theory the order parameter (P_s) is believed to fulfill the well known relation: $P_s \sim (T_c - T)^{\beta}$, the critical exponent was estimated to be ca. 0.52 which is characteristic (0.50–1.0) of the continuous ferroelectric phase transition (see inset in Fig. 9). We carried out also a pyroelectric experiment crossing the **III** → **IV** phase transition. The crystal was poled while cooling from 150 K down to 130 K with DC electric field as large as 8 kV/cm. Then the pyroelectric current was measured during cooling down to 100 K. It was found that the lowest temperature transition, **III** → **IV**, was pyroelectrically active, since it is accompanied by a significant decrease in the P_s magnitude by ca. 30%. Then the crystal, without any pooling field, was warmed through two phase transitions. The pyroelectric current and the spontaneous polarization vs. temperature between 120 and 150 K are illustrated in Fig. 11. It is clearly seen that the P_s experiences a visible increase at ca. 133 K (**IV** → **III**), which confirms the reversibility of the spontaneous polarization. Then the pyroelectric current shows a negative value with a strong peak attributed to the ferroelectric–paraelectric transition.

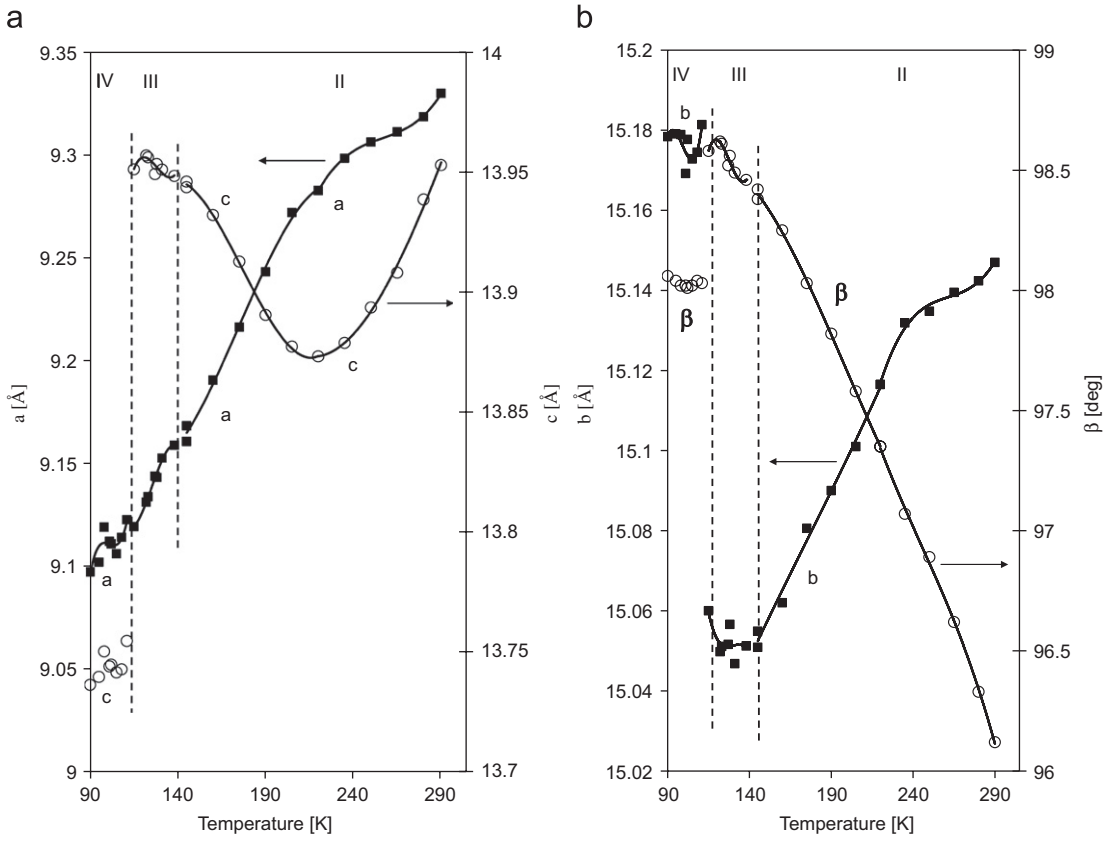

Fig. 6. Temperature dependencies of lattice parameters: (a) a and c and (b) b and monoclinic β angle.

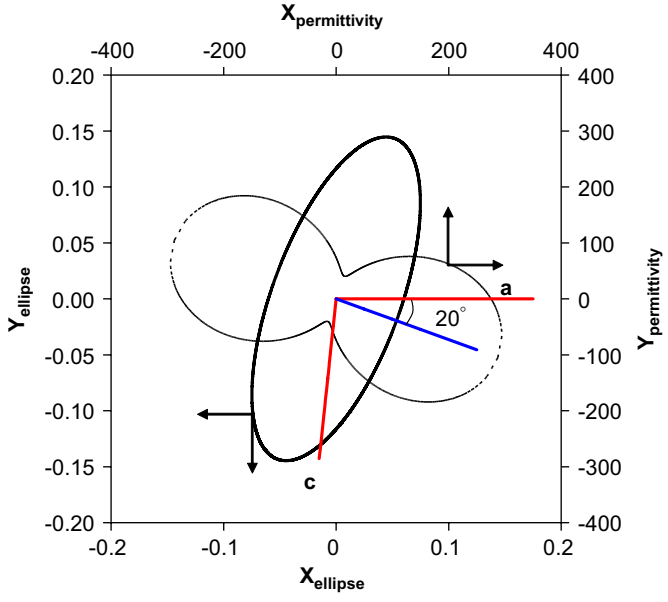

Fig. 7. Illustration of the geometric interpretation of the permittivity tensor. Solid line—ellipse, dotted line—directional dependence of permittivity.

It should be underlined that for some samples, upon heating starting from the lowest temperature phase **IV** the P_s magnitude is usually smaller than that found for the crystals which do not cross the **III** → **IV** transition temperature. It should be added that the **III** → **IV** transition is accompanied by a significant distortion of the lattice cell and additionally over all phases crystal possesses ferroelastic properties. These two features may affect on the reversibility of magnitudes of the electric permittivity and spontaneous polarization because of changes on the crystal surface and electric contacts. The pyroelectric measurements lead to the conclusion that both phase **III** and the lowest temperature phase **IV** have the ferroelectric properties.

$(C_3N_2H_5)_5Sb_2Br_{11}$ is characterized by a slow switching process and this is a reason that no ferroelectric hysteresis loop was observed using a Diamond–Dreck–Pepinsky bridge with an electric field of 50–10 Hz frequency. However, an application of markedly lower frequency (0.05 Hz) permits to observe a properly shaped hysteresis loops. The existence of the hysteresis loop below 145 K is a direct proof of a ferroelectricity in $(C_3N_2H_5)_5Sb_2Br_{11}$. The results of studies devoted to the switching of the spontaneous polarization will be presented in forthcoming publications.

The dielectric properties for all ferroelectric compounds, $R_5M_2X_{11}$ synthesized so far are summarized in Table 5.

In general all compounds crystallizing with $R_5M_2X_{11}$ chemical composition are characterized by large structural similarities. The common feature of them is the presence of five, divided into four nonequivalent types, organic cations

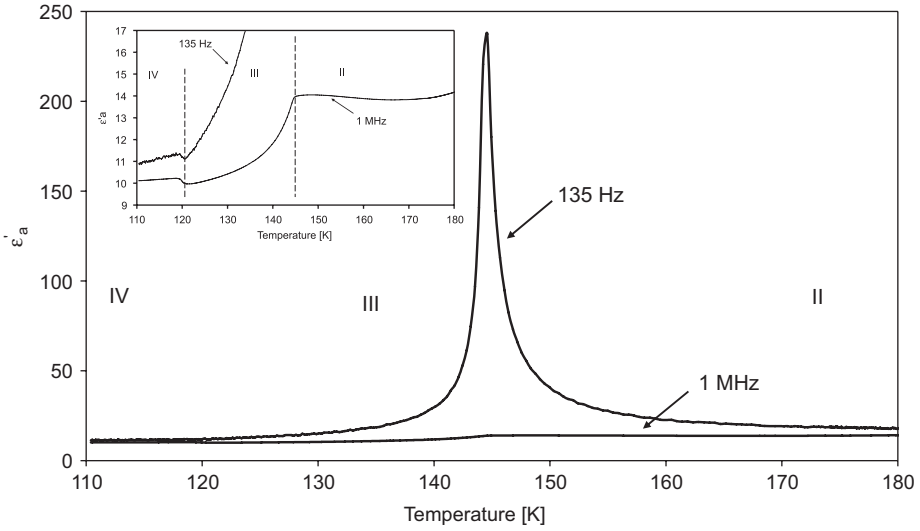

Fig. 8. Real part of the complex electric permittivity ε'_a, measured at the frequency 135 Hz and 1 MHz in the vicinity of the paraelectric–ferroelectric phase transition (**II** → **III**). The inset shows the temperature dependence of ε'_a at 135 Hz and 1 MHz in the vicinity of **III** → **IV** phase transition.

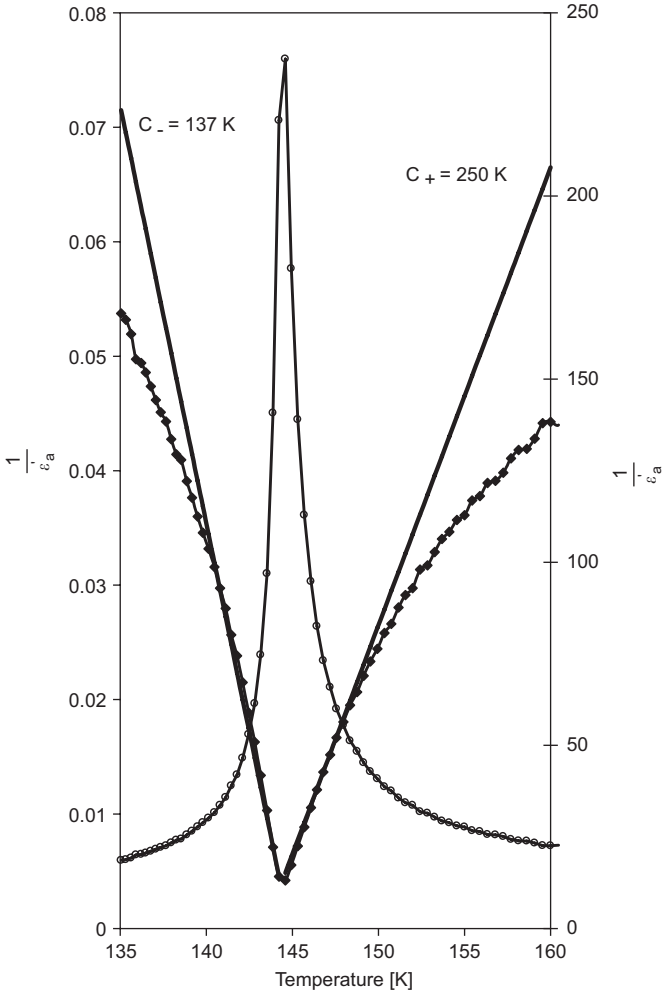

Fig. 9. $1/\varepsilon'_a$ *vs.* temperature representation (the Curie–Wess law).

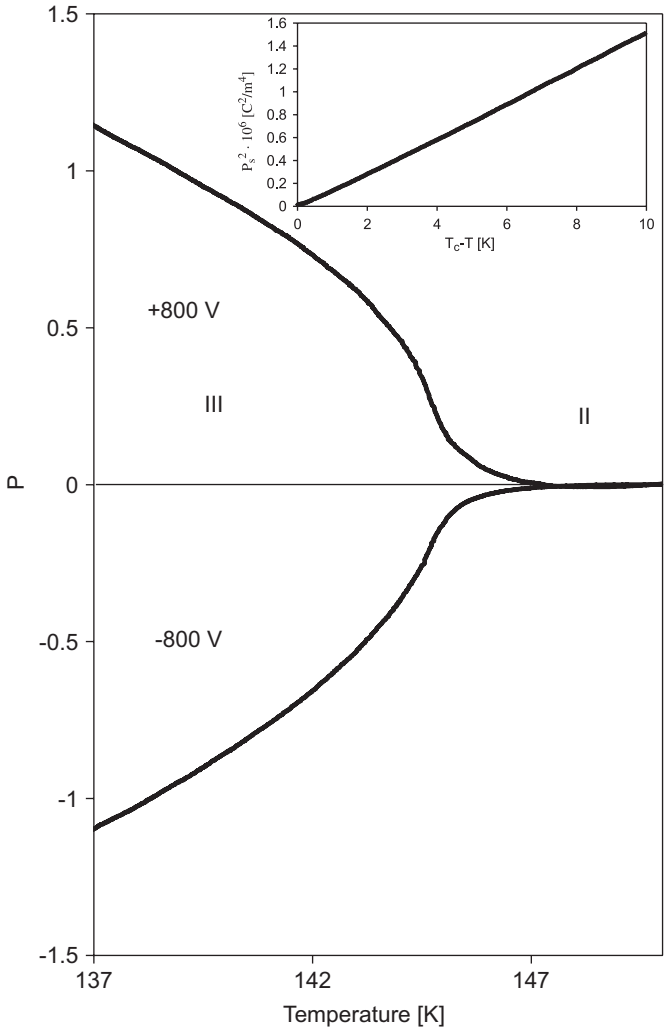

Fig. 10. Spontaneous polarization (P_s) as a function of temperature from the pyroelectric effect for the poling electric field 8 kV/cm over the ferroelectric phase **III**. The inset shows P_s^2 vs. $(T_c - T)$ in the vicinity of ferroelectric transition.

(methylammonium, pyridinium or imidazolium). In the paraelectric phases of all compounds, irrespective of the space group (*Pcab* or $P2_1/n$) among five cations two are

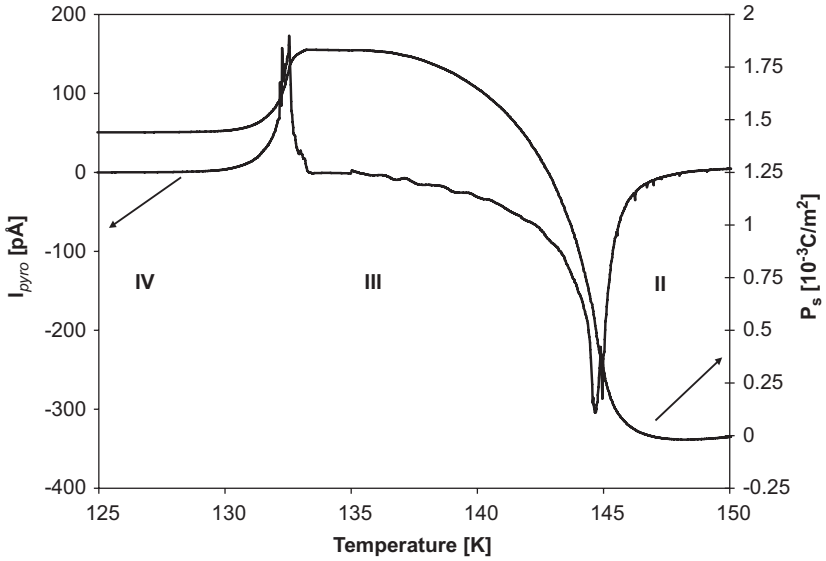

Fig. 11. Simultaneous spontaneous polarization and pyroelectric current, upon heating, over the temperature range covering two ferroelectric phases: **IV** and **III**. The sample was poled with electric field of 8 kV/cm from 150 to 130 K, and then cooled down to 100 K.

always ordered. The remaining three cations contribute to the ferroelectric phase transition mechanism. However, the ordering of the cations, which undergoes continuously with temperature over the ferroelectric phase, may be a little different in the methylammonium and imidazolium analogs, which is reflected in different phase situation. The other reason leading to the differentiation of the dielectric and polar properties of these two groups seems to be connected with the strength of interactions of dipolar cations. The dipole–dipole interactions in the methylammonium analogs are significantly stronger than those in the imidazolium ones, since the methylammonium cations are bestowed with the higher permanent dipole moment. It results in the higher values of T_c, as well as in the larger dielectric permittivity and spontaneous polarization in methylammonium analogs in comparison to those found for the imidazolium ones.

4. Conclusion

(1) Three solid–solid phase transitions are disclosed in the title crystal:
$(tetragonal?) \overset{354/352}{\longleftrightarrow} P2_1/n$ (**I**↔**II**) discontinuous?
$P2_1/n \overset{145}{\longleftrightarrow} Pn$ (**II**↔**III**) continuous,
$Pn \overset{120/135}{\longleftrightarrow} Pn$ (**III**↔**IV**) discontinuous, isomorphous.

(2) $(C_3N_2H_5)_2Sb_2Br_{11}$ was found to be a ferroelectric compound with the Curie point at 145 K and the saturated spontaneous polarization of ca. 1.8×10^{-3} C m^{-2}, which is characteristic of "weak" ferroelectric materials. The polar properties are extended over phases **III** and **IV**.

(3) The crystal structure of $(C_3N_2H_5)_2Sb_2Br_{11}$ consists of a discrete corner-sharing bioctahedra $Sb_2Br_{11}^{5-}$ and four kinds nonequivalent imidazolium cations (types A–D). In the paraelectric phase **II** the cations A are ordered , whereas B–D, highly disordered are distributed over two sites (occupancy 0.50/0.50). In the ferroelectric phase **III** the cations B and C become continuously ordered with temperature decreasing.

(4) The ferroelectric phase transition mechanism is governed by the dynamics of dipolar imidazolium cations (types B and C), which contribute predominantly to the spontaneous polarization and determine the dielectric permittivity function close to 145 K.

(5) The order–disorder mechanism of the paraelectric–ferroelectric transition is in full accord with the preliminary dielectric dispersion experiment which disclosed a critical slowing down of the relaxation process in the kilohertz frequency region in the vicinity of 145 K.

Acknowledgments

This work was supported by the Polish State Committee for Scientific Research (Project Register No. N204 108 31/2551).

References

[1] R. Jakubas, L. Sobczyk, Phase Transitions 20 (1990) 163–193.
[2] H. Ishihara, K. Watanabe, A. Iwata, K. Yanida, Y. Kinoshita, T. Okuda, V.G. Krishnan, S. Dou, A. Weiss, Z. Naturforsch 47 (1992) 65–74.
[3] T. Okuda, H. Ishihara, K. Yamada, A. Weiss, Bull. Chem. Soc. Jpn. 66 (1993) 380–383.
[4] R. Jakubas, L. Sobczyk, J. Zaleski, Pol. J. Chem. 71 (1997) 265–300.
[5] M. Bujak, J. Zaleski, Cryst. Eng. 4 (2001) 241–252.
[6] M. Iwata, Y. Ishibashi, Ferroelectrics 135 (1992) 283–289.
[7] J. Mróz, R. Jakubas, Ferroelectrics Lett. 17 (1994) 73–78.
[8] J. Zaleski, A. Pietraszko, Acta Crystallogr. B 52 (1996) 287–295.
[9] J. Zaleski, C. Pawlaczyk, R. Jakubas, H.-G. Unruh, J. Phys.: Condens. Matter 12 (2000) 7509–7521.
[10] M. Bujak, J. Zaleski, J. Sol. State Chem. 177 (2004) 3202–3211.

[11] R. Jakubas, A. Piecha, A. Pietraszko, G. Bator, Phys. Rev. B 72 (2005) 104107–104114.
[12] Oxford Diffraction, *CrysAlis* CCD and *CrysAlis* RED, ver. 171.32.6. Oxford Diffraction Ltd., Abingdon, England, 2007.
[13] G.M. Sheldrick, *SHELX*. Program for the solution and refinement of crystal structures, University of Göttingen, Germany, 1997.
[14] P. Carpentier, J. Lefebvre, R. Jakubas, Acta Crystallogr., Sect.B: Struct. Sci. 51 (1995) 167–174.
[15] A. Piecha, R. Jakubas, J. Phys.: Condens. Matter. 19 (1–8) (2007) 406225.
[16] A.Y. Kudzin, M.D. Volnianskii, I.A. Bsoul, Ferroelectrics 215 (1998) 23–30.
[17] P. Vanej, Z. Zikmund, K. Krupa, A. Pronin, S. Kamba, J. Petzelt, Solid State Commun. 105 (1998) 439–443.
[18] J. Lefebvre, P. Carpentier, R. Jakubas, L. Sobczyk, Phase Transitions 33 (1991) 31–41.
[19] C. Pawlaczyk, H. Motsch, R. Jakubas, H.G. Unruh, Ferroelectrics 108 (1998) 127–132.
[20] J. Mróz, R. Jakubas, Solid State Commun. 72 (1989) 813–816.
[21] J. Jóźków, G. Bator, R. Jakubas, A. Pietraszko, J. Chem. Phys. 114 (2001) 7239–7246.